Modulating the Voltage Decay and Cationic Redox Kinetics of Li-Rich Cathodes

Li-rich layered transition-metal-oxide cathodes with a lower fraction of the Li_2MnO_3 phase exhibit improved electrochemical performance in Li-ion batteries.

Li-rich layered transition-metal-oxide cathodes with a chemical formula of $Li_{1+x}(Ni,Co,Mn)_{1-x}O_2$ have attracted great attention, mainly due to their substantially high capacities for advanced Li-ion batteries (LIB). However, Li-rich cathodes are limited by oxygen release, voltage fade/hysteresis, and poor electrochemical kinetics during cycling, possibly resulting from the oxygen redox reaction. To mitigate the unfavorable electrochemical properties of Li-rich cathodes, it is imperative to establish the oxygen redox mechanism. Recently, Heng-Liang Wu (National Taiwan University), Maw-Kuen Wu (Academia Sinica) and their collaborators from the NSRRC investigated the charge-storage mechanism of Li-rich cathodes with different amounts of the Li_2MnO_3 phase and Ni using *operando* quick-scanning X-ray absorption spectroscopy (XAS) at **TPS 44A**, soft XAS at **TLS 20A1**, and *operando* X-ray diffraction at **TLS 01C2**. The unfavorable electrochemical properties of the Li-rich cathodes could be limited by optimizing the ratio of Li_2MnO_3 phase. The effect of excess Li on the reversibility of the cation and anion redox of Li-rich cathodes was discussed. Both the as-synthesized $Li_{1.2}Ni_{0.13}Co_{0.13}Mn_{0.54}O_2$ (HLC) and $Li_{1.08}Ni_{0.34}Co_{0.08}Mn_{0.5}O_2$ (LLC) materials exhibit similar crystal structures, albeit different electrochemical behaviors. LLC materials reveal that reversible cation/anion redox reactions and voltage decay can be suppressed during cycling. The cation oxidation of the LLC cathode is kinetically slower than that of the HLC cathode, suggesting that the local coordination structure exerts a considerable impact on the reaction kinetics. The mechanistic insights into the Li_2MnO_3 phase and electrochemical kinetics of cation and anion redox are indispensable for improving Li-rich cathodes.

Figures 1(a–c) show the differential capacity (dQ/dV) plots and electrochemical performance of HLC and LLC cathode materials. As compared to the intensity of peak B for the HLC cathode, the peak D with a weaker intensity possibly results from the low content of Li in the transition metal (TM) layer of LLC materials (**Figs. 1(a) and 1(b)**). The corresponding reduction peaks are shifted drastically toward the low-potential region for the HLC cathode (marked by the arrows), suggesting that voltage fading is more severe in HLC cathode than in the LLC cathode during cycling. **Figure 1(c)** shows that the electrochemical stability of the LLC cathode is improved. **Figures 2(a) and 2(b)** (see next page) show the representative *operando* Ni K-edge X-ray absorption spectra of the HLC and LLC cathodes in the first cycle. The Ni K-edge absorption energies of the HLC cathode and the corresponding charge-discharge curves are shown in **Figs. 2(c) and 2(d)**, respectively. At a potential of greater than 4.4 V, the oxidation state of Ni remains the same, which is consistent with the fact that the oxidation process is dominated by the anion (O^{2-}) oxidation process rather than the TM oxidation process at a high-potential region (> 4.4 V). During the discharge process, the Ni K-edge absorption energy shifts to a lower energy as a result of Ni reduction. The changes in the Ni K-edge absorption energy are monotonic during the discharge process, suggesting that anion and TM reduction processes could be performed at similar potentials. **Figures 2(e) and 2(f)** show the Ni K-edge absorption energies of the LLC cathode and the corresponding charge–discharge curves in the first cycle. Interestingly, the changes in Ni K-edge absorption energies yield two different slopes, which are indicated by dashed lines during the discharge process (**Fig.**

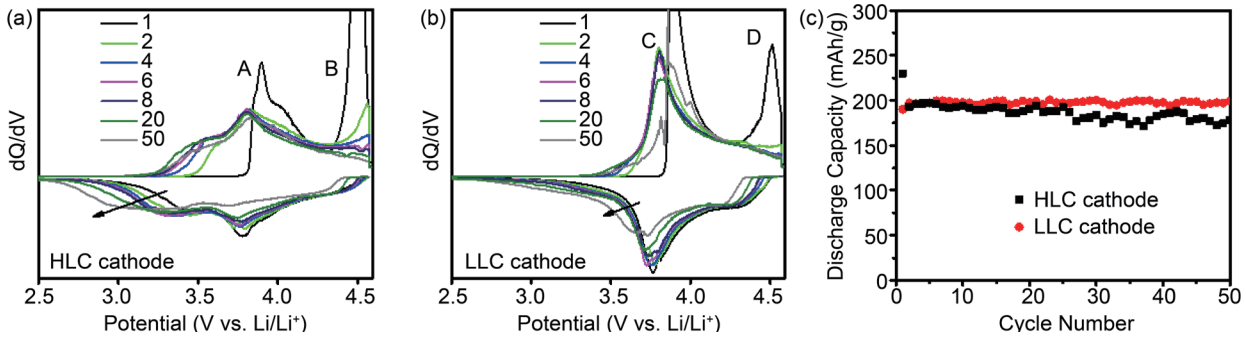

Fig. 1: dQ/dV plots of (a) HLC and (b) LLC cathode materials. (c) Electrochemical performance of LLC and HLC cathode materials obtained at a rate of 20 mA/g in a potential range of 4.6 to 2.2 V. [Reproduced from Ref. 1]

2(f)). The oxidation state of Ni is maintained from 4.6 V to 4.4 V, followed by substantial changes at potentials of less than 4.4 V, likely resulting from anion reduction and TM reduction processes, respectively. The 2D XAS mapping at the Ni K-edge on the HLC and LLC particles is recorded at 4.6 V and 4.4 V during discharge. The full charged state of Ni (Ni^{4+}) is distributed uniformly on the HLC particle at 4.6 V, which is consistent with *in operando* XAS results.

Figure 3(a) shows the proposed reaction mechanism of HLC and LLC cathodes, which will be discussed further, and the corresponding CV results. During the charge process, TM oxidation is performed (region I), followed by anion oxidation (region II) in both the HLC and LLC cathodes. Severe voltage decay is observed for the HLC cathode, and anion reduction occurs at a lower potential region along with TM reduction process. The LLC cathode exhibits sequential anion and TM reduction reactions during the discharge process. The TM layer is known to resemble a honeycomb-like structure, yielding a high amount of the Li_2MnO_3 phase (C2/m structure) in the HLC material. The lattice oxygen tends to form an oxygen dimer with short covalent bonds at a high-potential region during the delithiation process, which causes the metal-oxygen de-coordination and cation migration. The voltage decay could originate from the cation migration during the

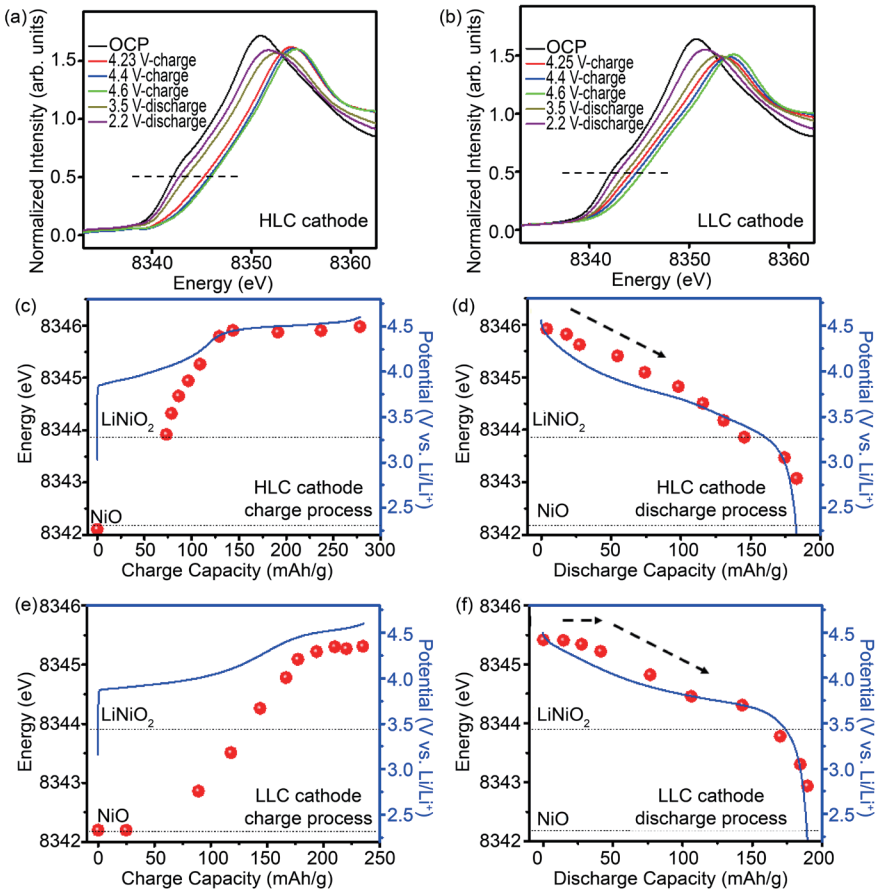

Fig. 2: *Operando* Ni K-edge X-ray absorption spectra of (a) HLC and (b) LLC cathodes during cycling. Ni K-edge absorption energies of (c,d) HLC and (e,f) LLC cathodes and their corresponding charge–discharge curves. The K-edge energies are evaluated at a normalized intensity of 0.5. [Reproduced from Ref. 1]

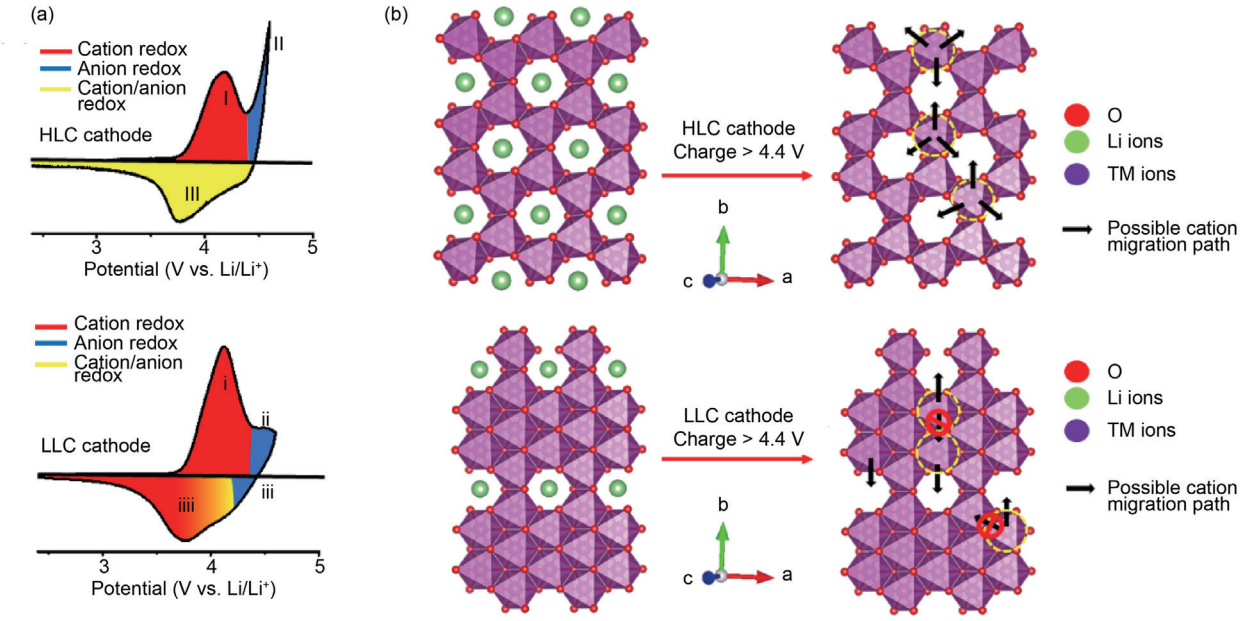

Fig. 3: (a) Reaction mechanism of HLC and LLC cathodes and the corresponding CV results. (b) Cation migration mechanism. Schematic of the cation migration in HLC and LLC cathodes. Colors for different elements: O is red, Li is green, and TM is purple. [Reproduced from Ref. 1]

lithiation process. **Figure 3(b)** shows a schematic of the cation migration mechanism in the HLC and LLC cathodes. Since the HLC cathode has more Li_2MnO_3 phases than the LLC cathode, cation migration is performed easily and the vacancies are clustered in the TM layer. Thus, the lattice oxygen with different coordination environments can cause shifts in the oxygen reduction potential and the occurrence of voltage fading during the lithiation process. There is a lower fraction of the Li_2MnO_3 phase in the LLC cathode, which limits the cation migration and suppresses the voltage fading. (Reported by Heng-Liang Wu, National Taiwan University)

This report features the work of Heng-Liang Wu, Maw-Kuen Wu and their collaborators published in Adv. Funct. Mater. ***32****, 2112394 (2022).*

TPS 44A Quick-scanning X-ray Absorption Spectroscopy
TLS 01C2 X-ray Powder Diffraction
TLS 20A1 XAS

- XANES, EXAFS, XAFS
- Materials Science, Physics, Energy Storage Devices, Battery Materials, Chemistry, Condensed-matter Physics, Functional Materials

Reference

1. H.-L. Yu, K. B. Ibrahim, P.-W. Chi, Y.-H. Su, W.-T. Chen, S.-C. Tseng, M.-T. Tang, C.-L. Chen, H.-Y. Tang, C.-W. Pao, K.-H. Chen, M.-K. Wu, H.-L. Wu, Adv. Funct. Mater. **32**, 2112394 (2022).

Charge–Discharge Mechanism of High-Entropy Co-Free Spinel Oxide in Li-ion Batteries

Li^+ storage mechanism of high-entropy Co-free spinel oxide was firstly evaluated using operando quick-scanning X-ray absorption spectroscopy.

Transition-metal high-entropy oxides (HEO) that integrate five (or more) elements into a single phase are considered as potential anodes for Li-ion batteries (LIB). Entropy-derived phase stabilization enhances the electrode reversibility and cyclic stability. Moreover, the HEO lattice is distorted because of the distinct atomic sizes of the constituents, which cause a lattice residual stress that can alter material properties. An as-synthesized cobalt-free spinel $(CrMnFeNiCu)_3O_4$ LIB anode is studied in this work. A homogeneous distribution of the constituent elements is verified by energy-dispersive X-ray spectroscopy mapping data and the K-edge k^3-weighted extended X-ray absorption fine structure (EXAFS) and Fourier-transform magnitude spectra, as shown in **Figs. 1(a) and 1(b)** (see next page). The galvanostatic charge–discharge profiles of the HEO anode exhibit a reversible specific capacity of 750 mAh g^{-1} at a rate of 50 mA g^{-1}. At a high rate of 2000 mA g^{-1}, a good specific capacity of 340 mAh g^{-1} is still achieved, corresponding to a satisfactory capacity retention of 45% compared to the value measured at 50 mA g^{-1} (**Fig. 1(c)**).

The multiple electroactive centers result in a complex Li^+ storage mechanism. The charge storage mechanism of HEOs appears to vary with their crystal structures and chemical composition and thus it is still disputed in the literature. The detailed HEO redox mechanism needs to be further examined to facilitate the design of electrode materials. Recently, Jeng-Kuei Chuang (National Yang Ming Chiao Tung University) and Chih-Wen Pao (NSRRC) explored the charge storage mechanism of a cobalt-free spinel $(CrMnFeNiCu)_3O_4$ HEO in detail by using *operando* quick-scanning X-ray absorption spectroscopy (XAS) of **TPS 44A**. XAS is sensitive to the local electronic structures of the absorbing atoms, making it suitable for investigation of the redox behavior of the HEO constituent elements. The XAS spectra are recorded in the transmission mode at a monochromator oscillation frequency of 2 Hz (*i.e.*, two complete spectra are recorded per second). A total of 240 spectra are integrated to achieve a good signal-to-noise ratio and a 2-min time resolution. This setup makes it feasible to investigate the detailed changes in the material and short-lived intermediate species formed during lithiation/delithiation. The valence/coordination state variations, multiple transition steps, redox sequence, reversibility, and redox overpotentials of Cr, Mn, Fe, Ni, and Cu species in the HEO electrode are examined, as illustrated in **Fig. 2** (see next page).

In pristine HEO, the cations are present as $Mn^{2+/3+}$, Cu^{2+}, Cr^{3+}, $Fe^{2+/3+}$, and Ni^{2+}, which are distributed at both the tetrahedral and octahedral sites. Upon the first lithiation (*i.e.*, charging), the $Mn^{2+/3+} \rightarrow Mn^{2+}$ and $Cu^{2+} \rightarrow Cu^0$ reactions contribute to the capacity in the potential sloping region. Then, the (Mn^{2+} and $Mn^{2+/3+}$) $\rightarrow Mn^0$, $Cr^{3+} \rightarrow Cr^{2+}$, $Fe^{2+/3+} \rightarrow Fe^{2+}$, $Fe^{2+} \rightarrow Fe^0$, and